Flexural wave propagation in rigid elastic combined metabeam

Abhigna Bhatt
Department of Civil Engineering
Indian Institute of Technology Delhi
Email: abhigna.bhatt@gmail.com

Arnab Banerjee
Department of Civil Engineering
Indian Institute of Technology Delhi
Email: abanerjee@iitd.ac.in

Abstract: In this paper, flexural wave propagation, attenuation and reflection through finite number of rigid elastic combined meta-beam (RECM) elements sandwiched between two Euler Bernoulli beams has been studied, implementing the spectral element, inverse Fourier transform and transfer matrix method. Spectral element has been formulated for the unit representative cell of RECM employing the rigid-body dynamics. Governing dimensionless parameters are identified. Further, the sensitivity analysis has been carried out to comprehend the influence of non-dimensional parameters such as mass ratio, length ratio, and rotary inertia ratio on the attenuation profile. Rotary inertia of rigid body produces Local resonance(LR) band, which may abridge the gap between the two Bragg Scattering(BS) bands and results in an ultra-wide stop-band for the specific combination of governing non-dimensional parameters. 164% normalized attenuation band is possible to obtain in RECM. Natural frequencies for the finite RECM have also been evaluated from the global spectral element matrix and observed that some natural frequencies lies in the attenuation band. Therefore, the level of attenuation near that natural frequencies is significantly less and cannot be identified from the dispersion diagram of the infinite RECM.

Keywords: Spectral element method; Rigid body dynamics; Transfer matrix; Dispersion relationship; Band structure; Attenuation profile

1 Introduction

In the past few decades, the study of flexural wave propagation through periodic structures has gained assiduity because of its ability to filter out unwanted frequencies [1,2,3,4,5,6]. Depending on properties of the representative unit cell, wave of some frequency may propagate (pass or propagation band) and some may attenuate (stop or attenuation band) [7]. This correlation between excitation frequency and wave number is called dispersion relationship [8]. The dispersion relationship can be characterized from the constituents of the representative unit cell like stiffness, damping, mass etc [9]. Bragg scattering (BS) [10], local resonance (LR) [11] and inertial amplification (IA) [12] are primary mechanisms of stop band creation. BS band occurs due to negative interference; whereas, LR band originates due to out of phase resonance in a beam [13]. The need of wider bandwidth has driven the research towards the merging of several band-gaps originated from the different physics, such as, use of inertia [14], inertial amplifier [15], periodic resonators [16,17,18,19], negative stiffness [20] etc. The band structure characteristic in infinitely long beam incorporating non-linearity [21], linear variation in mass and stiffness [22, 23], geometric variation in beam [10] etc has been explored in the past. However, no study in the field of wave propagation through the rigid elastic combined metabeam(RECM) considering the finite dimension of the rigid mass was reported.

In this paper, the band structure characteristics for infinitely long RECM, as shown in Figure 1(a), is studied. The dispersion relationship of one-dimensional periodic structures can be obtained very efficiently by evaluating logarithms of eigenvalues of the transfer matrix of the representative cell [18]. To obtain the transfer matrix, the exact analytical solution of a periodic cell has been obtained using spectral element method [24, 25, 26].

The rigid-elastic combination were established adopting the conventional assembling techniques of spectral element matrix or dynamics stiffness matrix [27, 28, 29, 30, 31] and finite element method [32]. The representative unit cell is considered as illustrated in Figure 1(b). The displacement continuity and force equilibrium equations in rigid body is calculated to obtain condensed spectral element matrix. To validate the spectral element formulation, a repeating unit cell has been considered as illustrated in Figure 4(a) and its modal frequencies were matched with solution obtained by reference [28]. The obtained spectral element matrix has been converted into transfer matrix to get the band struc-

ture. The influence of the nondimentional parameters of rigid body on band structure characteristics of RECM beam has been investigated in this study. The finite system of a few RECM elements has been constructed to get the frequency response function (FRF). Study of both finite and infinite structures unable us to get the detailed understanding of attenuation characteristics. Further, The flexural wave propagation through two Euler Bernoulli beams connected by eight RECM elements is analysed and using inverse Fourier transform the space-time response is plotted to visualise the wave dispersion. Development of analytical expression for the spectral element matrix of RECM unit cell, observation of the natural frequencies in the attenuation band and visualization of the flexural dispersive wave propagation, attenuation and reflection through RECM are the salient attributes of the paper.

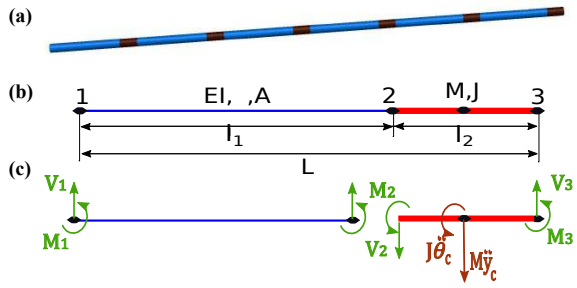

Fig. 1: (a) The Infinite Rigid Elastic combined meta(RECM) beam, (b) The representative unit cell of RECM beam (where, EI is flexural rigidity, A is area of cross section, l_1 and l_2 are lengths of elastic and rigid part of beam respectively, M is mass and J is rotary inertia of rigid body and L is total length of a unit cell)and (c) Free body diagram of unit cell of RECM beam (where, M_i and V_i are moment and shear force at i^{th} node, θ_c and y_c are slope and displacement at the center of rigid body)

2 Methodology

The representative unit cell (Figure 1(b)) has two elements, first is elastic beam element of length l_1, connected by node 1-2 and another is rigid body of length l_2, connected by node 2-3. As it is a beam element each node has two degrees of freedom, vertical displacement and rotation. vertical displacement in upward direction and rotation in anti clockwise direction is assumed to be positive.

2.1 Governing equation

The elastic part of beam is assumed to be following Euler Bernoulli beam theory. The governing elastic beam equation can be written as:

$$EI\frac{\partial^4\tilde{w}}{\partial\tilde{z}^4}+\rho A\frac{\partial^2\tilde{w}}{\partial\tilde{t}^2}=0 \tag{1}$$

where, $\tilde{w}$ denotes deflection in $\tilde{z}$ (transverse) axis and $\tilde{t}$ represents time. For obtaining non-dimensional equations, substituting $\tilde{z}=zl_1$, $t=\omega_n\tilde{t}$, $\tilde{w}=W\,w(z,t)$ (W is an arbitrary constant), $\omega_n^2=EI/\rho Al_1^4$, $\eta=\omega/\omega_n$ and the solution is assumed to be $w(\tilde{z},t)=Y(z)e^{i\eta t}$ in Equation 1. [18]. The beam equation can be obtained as a spacial ODE as:

$$Y^{IV}(z)-\eta^2Y(z)=0 \tag{2}$$

The general solution of spacial ODE is considered as:

$$Y(z)=\phi(z)C \tag{3}$$

where, $\lambda=\sqrt{\eta}$, $C=\left\{C_1\ C_2\ C_3\ C_4\right\}^T$ and $\phi(z)=[\cos(\lambda z)\ \sin(\lambda z)\ \cosh(\lambda z)\ \sinh(\lambda z)]$

2.2 Spectral element formulation

Spectral element matrix(SEM) of representative unit cell has been formulated by first developing SEM of elastic part of RECM [25]. Each node of beam has four states: displacement $y(z)$, slope $\theta(z)$, bending moment $M(z)$ and shear force $V(z)$. That are defined as follows:

$$y(z)=Y(z),\theta(z)=\frac{1}{l_1}Y'(z),$$
$$M(z)=\frac{EI}{l_1^2}Y''(z),V(z)=\frac{EI}{l_1^3}Y'''(z) \tag{4}$$

The spectral nodal displacement and slope can be related to displacement field by

$$U=HC\Longrightarrow C=H^{-1}U \tag{5}$$

where, $U=\left\{y_1\ \theta_1\ y_2\ \theta_2\right\}^T$ and

$$H=\begin{bmatrix}1 & 0 & 1 & 0\\ 0 & \frac{\lambda}{l_1} & 0 & \frac{\lambda}{l_1}\\ \cos(\lambda) & \sin(\lambda) & \cosh(\lambda) & \sinh(\lambda)\\ -\frac{\sin(\lambda)\lambda}{l_1} & \frac{\cos(\lambda)\lambda}{l_1} & \frac{\sinh(\lambda)\lambda}{l_1} & \frac{\lambda\cosh(\lambda)}{l_1}\end{bmatrix}$$

The shape function for displacement can be obtained by substituting constant vector C from Equation 5 in to Equation 3.

$$Y(z)=N(z)U \tag{6}$$

where, shape function $N(z)=\phi(z)H^{-1}$.The nodal forces can be defined as

$$F=\left\{V_1\ M_1\ V_2\ M_2\right\}^T$$
$$=\left\{V(0)\ -M(0)\ -V(1)\ M(1)\right\}^T \tag{7}$$

Now, Equation 4 can be substituted in Equation 7 to obtain the spectral element equation $F = SU$ of elastic beam. Where, spectral element matrix,

$$S = f \begin{bmatrix} S_{11} & S_{12} & S_{13} & S_{14} \\ S_{12} & S_{22} & -S_{14} & S_{24} \\ S_{13} & -S_{14} & S_{11} & -S_{12} \\ S_{14} & S_{24} & -S_{12} & S_{22} \end{bmatrix} \tag{8}$$

in which, $f = \frac{EI}{{l_1}^3(1-cch)}$, $S_{11} = \lambda^3(shc+chs)$, $S_{12} = l_1\lambda^2 shs$,
$S_{13} = -\lambda^3(sh+s)$,
$S_{14} = -l_1\lambda^2(c-ch)$, $S_{22} = -{l_1}^2\lambda(shc-chs)$,
$S_{24} = -{l_1}^2\lambda(s-sh)$, $c = \cos(\lambda)$, $ch = \cosh(\lambda)$,
$s = \sin(\lambda)$, $sh = \sinh(\lambda)$.
The concept of rigid body dynamics can be applied from the free body diagram illustrated in Figure 1(c). The relation between states of node 2 and node 3 can be defined using compatibility and force equilibrium equations. The equation of displacement and rotation compatibility condition is as follows:

$$\begin{Bmatrix} y_2 \\ \theta_2 \end{Bmatrix} = \begin{bmatrix} 1 & -l_2 \\ 0 & 1 \end{bmatrix} \begin{Bmatrix} y_3 \\ \theta_3 \end{Bmatrix} \tag{9}$$

The dynamic equation for force equilibrium can be written as follows:

$$\begin{Bmatrix} V_3 \\ M_3 \end{Bmatrix} = \begin{bmatrix} 1 & 0 \\ -l_2 & 1 \end{bmatrix} \begin{Bmatrix} V_2 \\ M_2 \end{Bmatrix} - \omega_n^2\lambda^4 \begin{bmatrix} m & -\frac{ml_2}{2} \\ -\frac{ml_2}{2} & J+\frac{{ml_2}^2}{4} \end{bmatrix} \begin{Bmatrix} y_3 \\ \theta_3 \end{Bmatrix} \tag{10}$$

The dimensionless parameters length ratio $\xi = l_2/l_1$, mass ratio $\mu = M/\rho A l_1$ and rotary inertia ratio $\Psi = J/Ml_2^2$ has been substituted in the equations 8, 9 and 10 to obtain non-dimensional spectral element. Knowing the relation between all states of nodes 1, 2 and 3; the spectral element of complete representative unit cell (Figure 1(b)) can be obtained as Equation 11.

$$\begin{Bmatrix} V_1 \\ M_1 \\ V_3 \\ M_3 \end{Bmatrix} = K \begin{Bmatrix} y_1 \\ \theta_1 \\ y_3 \\ \theta_3 \end{Bmatrix} \tag{11}$$

where, The spectral element matrix,

$$K = f \begin{bmatrix} K_{11} & K_{12} & K_{13} & K_{14} \\ K_{12} & K_{22} & K_{23} & K_{24} \\ K_{13} & K_{23} & K_{33} & K_{34} \\ K_{14} & K_{24} & K_{34} & K_{44} \end{bmatrix} \tag{12}$$

$$\begin{aligned}
&K_{11} = \lambda^3(shc+chs), K_{12} = l_1\lambda^2 shs, \\
&K_{13} = -\lambda^3(sh+s), K_{14} = -\xi K_{13} - K_{23}, \\
&K_{22} = -l_1^2\lambda(shc-chs), K_{23} = l_1\lambda^2(-ch+c), \\
&K_{24} = -\xi l_1 K_{23} - \lambda(-sh+s){l_1}^2, \\
&K_{33} = \lambda^3\left(\mu(cch-1)\lambda\right) + K_{11}, \\
&K_{34} = -l_1\lambda^2\left(\frac{\mu\xi(cch-1)\lambda^2}{2}\right) - l_1\xi K_{11} - K_{12}, \\
&K_{44} = l_1^2\lambda\left(\left(\psi+\frac{1}{4}\right)\mu(cch-1)\xi^2\lambda^3\right) \\
&\quad + l_1^2\xi^2 K_{11} + 2\xi l_1 K_{12} + K_{22}
\end{aligned}$$

2.3 Dispersion relation

The dispersion relationship can be computed very easily by solving eigen values of a transfer matrix. The transfer matrix is a matrix relating the states of end nodes of a representative unit cell. The spectral element matrix given in Equation 12 can be converted to transfer matrix T_s by [25]:

$$T_s = \begin{bmatrix} -K_{LR}^{-1}K_{LL} & -{K_{LR}}^{-1} \\ K_{RL} - K_{RR}{K_{LR}}^{-1}K_{LL} & -K_{RR}{K_{LR}}^{-1} \end{bmatrix} \tag{13}$$

where, $K_{LL} = \begin{bmatrix} K_{11} & K_{12} \\ K_{21} & K_{22} \end{bmatrix}$, similarly K_{LR}, K_{RL} and K_{RR} are three quadrants of spectral element matrix K.
From Equation 14 and 15, following eigenvalue problem can be obtained [18]. The wave number corresponding to frequency ratio can be easily determined from transfer matrix using Bloch-Floquet's theorem (Equation 14).

$$\varepsilon_n(1) = e^{-i\kappa}I\varepsilon_{n-1}(1) \rightarrow \varepsilon_n(1) = e^{-i\kappa}I\varepsilon_n(3) \tag{14}$$

where, $\varepsilon_n(i) = \left\{ y_i \ \theta_i \ V_i \ M_i \right\}^T$ is vector of states of element n at node i. The relation between states of node 1 and 3 can be written in matrix form using transfer matrix as:

$$\varepsilon_n(1) = T_s\varepsilon_n(3) \tag{15}$$

From Equation 14 and Equation 16, the dispersion relation can be obtained as:

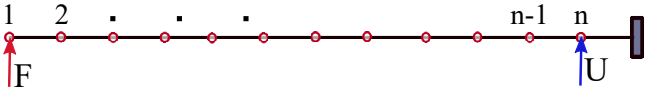

Fig. 2: Finite RECM beam chain

$$|T_s - e^{-i\kappa} I| = 0 \rightarrow \kappa = i\ln(eig(T_s)) \tag{16}$$

The total degrees of freedom of a unit cell is four but after applying Bloch's theorem it has been reduced to two. Therefor, the dispersion relation Equation 16 gives two pairs of complex conjugate values of wave number κ for corresponding frequency ratio η ($\eta = \lambda^2$). The dispersion characteristics depending on real and imaginary part of κ can be determined as propagation band, stop band, Bragg scattering or local resonance [18]. The imaginary value of wave number defines the level of attenuation.

2.4 Frequency domain response of Finite RECM system

In case of unsymmetrical and multi coupled element, the natural frequencies of the system may or may not occur in stop band [33]. It is interesting to see the effect of the natural frequencies present in the finite system and specifically within the stop band on the wave attenuation. For mono-coupled system, it is evident that frequency response plot has series of peaks in propagation band and a drop in the attenuation band. (cite - mead-1, A ban Jap 2017).

For detailed study of behaviour of RECM element, the cantilever beam is constructed using n RECM elements as displayed in Figure 2. The global SEM (K_g) of this system can be derived by assembling n SEM of RECM beam and applying cantilever boundary conditions to it. The receptance matrix (α) of the system can be obtained by inverting global SEM (K_g). The Frequency Response Function (FRF) for i^{th} degree of freedom (dof) due to force at j^{th} dof can be obtained from α_{ij} component of the receptance matrix [34].

$$\alpha_{ij} = \frac{U_i}{F_j} \tag{17}$$

The natural frequencies of the system can be obtained by equating determinant of global SEM equal to zero ($|K_g| = 0$).

2.5 Visualisation of wave propagation in space and time

To visualise the elastic wave propagation and comprehend the attenuation characteristics through any medium, the time domain response due to an excitation pulse need to be evaluated. Wave burst of having frequencies of interest can be generated to excite the system at one end for observing its propagation through the elastic medium. Then the generated excitation wave can be converted into frequency domain by Fourier transform. The spectral elements of elastic beam $S_e(\omega)$ and RECM beam $K(\omega)$ is derived in above

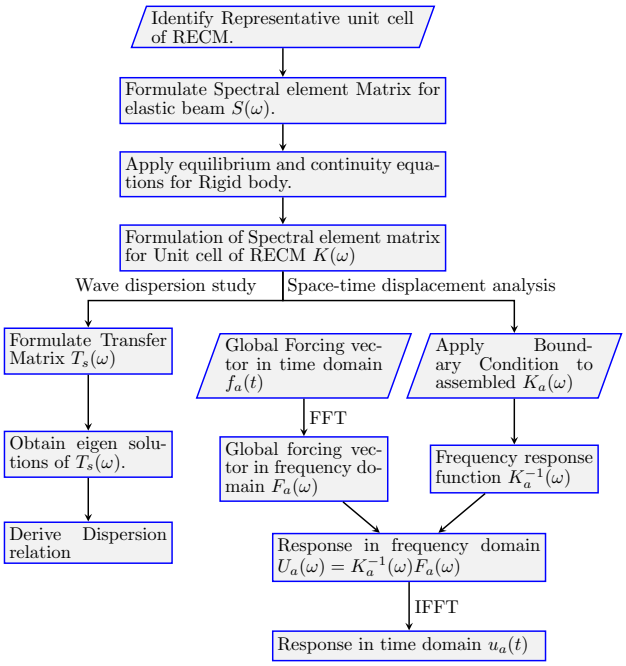

Fig. 3: Procedure for obtaining band characteristics and response in space-time domain for RECM beam

section. The global spectral element for the complete system $(K_a(\omega))$ can be obtained by assembly method similar to FEM (Finite Element Method). The excitation wave in frequency domain is used as the global force vector $(F_a(\omega))$ to obtain the response vector $(U_a(\omega))$ in frequency domain as given in Equation 18.

$$F_a(\omega) = K_a(\omega)U_a(\omega) \rightarrow U_a(\omega) = K_a^{-1}(\omega)F_a(\omega) \tag{18}$$

By applying Inverse Fast Fourier transform (IFFT) to response vector $(U_a(\omega))$, the response vector in time domain $(u_a(t))$ can be computed [25]. The overall process for obtaining band characteristic of series of RECM elements and visualization of wave propagation is elucidated in flowchart(Figure 3).

3 Validation

The different representative unit cells of the infinite beam would have same band structure formation but different spectral element matrix. In this section; spectral element matrix is formulated for another unit representative cell shown in Figure 4(a) to evaluate its natural frequencies for simply supported boundary conditions. The obtained solution is validated with the solution produced in paper [28]. Elastic beam connected by node 1-2 is beam 1 and another connected by node 4-5 is beam 2. The spectral element for

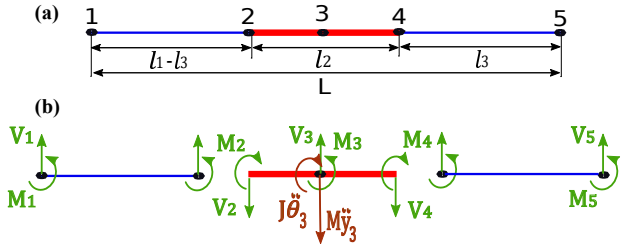

Fig. 4: (a) The representative unit cell of RECM beam for validation purpose and (b) Free body diagram of unit cell of RECM beam

them is uncoupled as per given in Equation 19.

$$\begin{Bmatrix} F_1 \\ F_2 \end{Bmatrix} = \begin{bmatrix} S_1 & O \\ O & S_2 \end{bmatrix} \begin{Bmatrix} U_1 \\ U_2 \end{Bmatrix} \tag{19}$$

Node 2 and 4 is connected by a rigid body so their relation with node 3 can be obtained by continuity and force equilibrium equations obtained from rigid body dynamics given in Figure 4(b).

Compatibility condition in matrix form:

$$\begin{bmatrix} y_2 \\ \theta_2 \\ y_4 \\ \theta_4 \end{bmatrix} = \underbrace{\begin{bmatrix} 1 & -\frac{l_2}{2} \\ 0 & 1 \\ 1 & \frac{l_2}{2} \\ 0 & 1 \end{bmatrix}}_{T} \begin{bmatrix} y_3 \\ \theta_3 \end{bmatrix} \tag{20}$$

Force equilibrium in matrix form:

$$\begin{bmatrix} V_3 \\ M_3 \end{bmatrix} = T' \begin{bmatrix} V_2 \\ M_2 \\ V_4 \\ M_4 \end{bmatrix} - \omega_n^2 \lambda^4 \begin{bmatrix} y_3 \\ \theta_3 \end{bmatrix} \tag{21}$$

The relation between the states of nodes 1,2,3,4 and 5 obtained in equations 22, 20 and 21 can be manipulated to obtain the spectral element Equation 22 of complete representative unit cell illustrated in Figure 4(a). The nondimentional parameters length ratio $\xi = l_2/l_1$, mass ratio $\mu = M/\rho A l_1$ and rotary inertia ratio $\Psi = J/Ml_2^2$ has been substituted the spectral element matrix $K_{6\times6}$.

$$\begin{bmatrix} V_1 & M_1 & V_3 & M_3 & V_5 & M_5 \end{bmatrix}' = K_{6\times6} \begin{bmatrix} y_1 & \theta_1 & y_3 & \theta_3 & y_5 & \theta_5 \end{bmatrix}' \tag{22}$$

Table 1: Natural frequency ω_n for combined elastic rigid beam with properties - $l_1 = 0.8L$, $l_2 = 0.2L$, $l_3 = 0.3L$, $\psi = 0$, $\mu = 0.5$ and $\xi = 0.5$

Mode	Natural frequency		Error (%)
	SEM	Ref [28]	
1	10.758	10.758	0
2	43.389	43.389	0
3	100.92	100.92	0

To validate the proposed algorithm, simply supported boundary condition are applied in Equation 22. The natural frequencies obtained from proposed spectral element matrix and calculated in reference [28] are found to be of exact match. The first three modal frequencies of one example problem from the paper [28] are matched with modal frequencies obtained from the present approach is given in Table 1. As both the methods are exact method, the zero error in calculation depicts perfect implementation of spectral element method. Dispersion relationship is found to be same for both the representative unit cell which validates the spectral element formulation of first unit cell (Figure 1(b)).

4 Results and Discussion

4.1 Study of the dispersion characteristics and natural frequencies

The dispersion relationship is invariant to the change in dimensional parameters, i.e., density, flexural rigidity, length and area of elastic body. Sensitivity analysis of the dispersion characteristics for an infinite number of RECM elements and the natural frequencies and frequency response of the finite (ten) number of RECM elements to the modification in nondimentional parameters, viz., length ratio (ξ), mass ratio (μ) and rotary inertia ratio (ψ) has been performed. The wave attenuates spatially while the minimum value of the attenuation constants $min(|\Im(\kappa)|$ is non-zero [11]. In this study, the contour plot of minimum attenuation constant ($min(|\Im(\kappa)|)$), termed as attenuation profile, is plotted for the range of natural frequency ratio ($0 < \eta \leq 50$). Among the three non-dimensional parameters, viz., length ratio (ξ), mass ratio (μ) and rotary inertia ratio (ψ), two parameters are kept constant and the remaining one varied in each attenuation profile plot to comprehend its influence. To provide an insight about the dispersion diagram (concise band structure) and frequency response function for ten units, a typical configuration has been chosen.

4.1.1 Variation of length ratio with zero rotary inertia

The Figure 5(a) presents the attenuation profile for varying length ratio ξ, having mass ratio $\mu = 0.25$ and rotary inertia $\psi = 0$. In Figure 5(b), the concise band structure for $\xi = 1$ is plotted. The symmetric nature of the profile of stop bands, as illustrated in Figure 5(b), explains the exis-

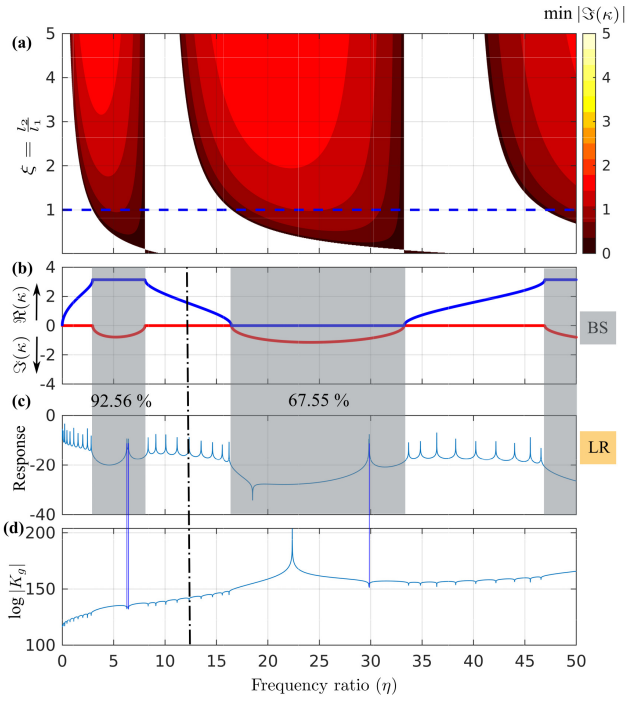

Fig. 5: (a)Attenuation-profile for varying length ratio ξ having rotary inertia ratio $\psi = 0$ and mass ratio $\mu = 0.25$. For the system parameters corresponds to $\psi = 0$, $\mu = 0.25$ and $\xi = 1$ - (b) concise dispersion diagram illustrating the attenuation and propagation bands and (c) plot of the cross frequency response function evidenced the reduction of response in the attenuation band. The normalised band width of first and second band is 92.56% and 67.56% respectively. (d) Plot of logarithmic determinant of global Spectral element Matrix, where downward peak corresponds to the natural frequency of the system. The thin blue lines connecting resonance peaks in (c) and downward peak in (d) illustrate occurrence of resonance peaks in the stop band. The vertical black center line indicates the mid frequency ratio (12.5) for the wave burst for visualization of displacement in space time.

tence of Bragg scattering [11]. The range of frequency ratio of first and second Bragg band are respectively $2.96 - 8.06$ (BWI 92.56%)and $16.46 - 33.25$ (BWI 67.56%). The drops in the cross frequency response function (FRF) Figure 5(c) matches pretty well with the stop bands. The resonance at the natural frequencies of the finite structure yields the series of peaks in pass band. Surprisingly, four peaks at frequency ratios 6.29, 6.43, 29.82 and 29.86 can be noticed in the cross FRF depicted in Figure 5(c). Also at this frequencies the attenuation level reduces in case of finite structure, however this information can not be obtained from the dispersion diagram of the infinite structure. Figure 5(d) is the plot of logarithmic determinant of global SEM (K_g) and the downward peaks in the plot depicts the natural frequencies of the system because at natural frequency the determinant of spectral element matrix will be zero so its log will be $-\infty$. Thin blue lines in Figure 5 connects resonance peaks in stop band with natural frequencies.

4.1.2 Variation of length ratio with non-zero rotary inertia

To investigate the effect of rotary inertia, attenuation profile for varying length ratio ξ having rotary inertia ratio $\psi = 5$ and mass ratio $\mu = 0.25$ is illustrated in Figure 6(a). Here, the merging of bands is visible at a particular length ratio ξ. The band structure and associated frequency response function at specific length ratio where merging occurs are elucidates Figure 6(b) and Figure 6(c). Sudden presence of LR band is noticed which abridged the two Bragg bands in Figure 6(b). The high attenuating response in LR band with anti-resonance peaks is clear in cross FRF Figure 6(c). The first band gap due to the merging phenomenon is obtained in range of frequency ratio 2.62-26.54 (BWI = 164%). At the merging point the attenuation level is very low due to the appearance of natural frequency. Natural frequencies of this system can be found out in Figure 6(d) which are exactly positioned at corresponding resonance peak in stop band but the anti-resonance (downward peaks in Figure 6(c)) has no direct relation with the natural frequencies of the system.

4.1.3 Variation of mass ratio with non-zero rotary inertia

The influence of mass ratio μ of RECM having length ratio $\xi = 0.5$ and rotary inertia ratio $\psi = 5$, on attenuation profile is illustrated in Figure 7(a). The band merging of first and second band can be observed at $\mu = 0.32$. The band structure and cross FRF for rotary inertia ratio $\psi = 5$, mass ratio $\mu = 0.32$ and length ratio $\xi = 0.5$ is illustrated in Figure 7(b) and Figure 7(c). The merged band gap range is found to be of frequency ratio 2.62-26.02 (BWI = 163.41 %). The cross FRF verifies the band structure characteristics by showing continuous response reduction in Bragg band and vibrating attenuation in LR band. The first stop band has peak response at frequency ratio 6.47 and 6.68 and at these same frequency ratios the downward peaks showing natural frequencies can be observed in Figure 7(d). .

4.1.4 Variation of rotary inertia ratio

The attenuation profile depicting the effect of relative polar moment of inertia of rigid body on dispersion relationship of RECM having mass ratio $\mu = 0.25$ and length ratio $\xi = 0.5$, is illustrated in Figure 8(a). At rotary inertia ratio $\psi = 1.71$, the merging of second and third band can be noticed. In Figure 8(b), the band structure of infinite RECM having rotary inertia ratio $\psi = 1.71$, mass ratio $\mu = 0.25$ and length ratio $\xi = 0.5$ is represented to show the merging of two Bragg bands with LR band distinctly. The Figure 8(c) delineates the cross FRF to verify the obtained band structure. The range of merged attenuation band is of frequency ratio 13.69-72.06 (BWI=136.14 %). The natural frequencies observed in Figure 8(d) correlate exactly with resonance peaks in FRF.

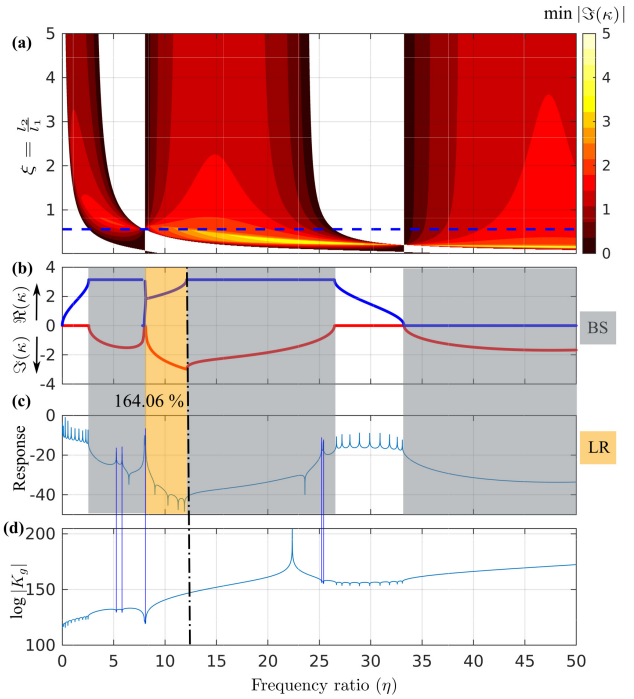

Fig. 6: (a)Attenuation-profile for varying length ratio ξ having rotary inertia ratio $\psi = 5$ and mass ratio $\mu = 0.25$. For the system parameters corresponds to $\psi = 5$, $\mu = 0.25$ and $\xi = 0.56$ - (b) concise dispersion diagram illustrating the attenuation and propagation bands and (c) plot of the cross frequency response function evidenced the reduction of response in the attenuation band. The normalised band width of first merged band is 164.06% (d) Plot of logarithmic determinant of global Spectral element Matrix, where downward peak corresponds to the natural frequency of the system. The thin blue lines connecting resonance peaks in (c) and downward peak in (d) illustrate occurrence of resonance peaks in the stop band. The vertical black center line indicates the mid frequency ratio (12.5) for the wave burst for visualization of displacement in space time.

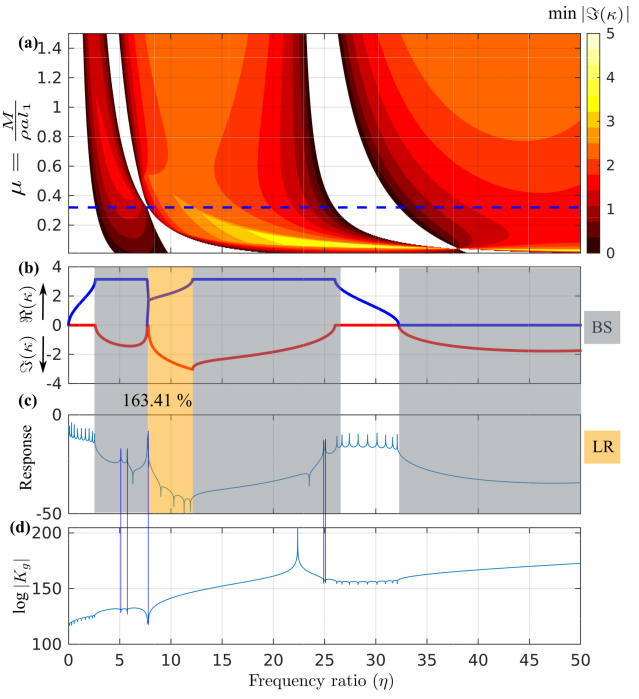

Fig. 7: (a)Attenuation-profile for varying mass ratio μ having rotary inertia ratio $\psi = 5$ and length ratio $\xi = 0.5$. For the system parameters corresponds to $\psi = 5$, $\mu = 0.32$ and $\xi = 0.5$ - (b) concise dispersion diagram illustrating the attenuation and propagation bands and (c) plot of the cross frequency response function evidenced the reduction of response in the attenuation band. The normalised band width of first merged band is 163.41% (d) Plot of logarithmic determinant of global Spectral element Matrix, where downward peak corresponds to the natural frequency of the system. The thin blue lines connecting resonance peaks in (c) and downward peak in (d) illustrate occurrence of resonance peaks in the stop band.

4.1.5 Concluding remarks

The Peak responses presents in the attenuation band are the result of existence of natural frequencies within the stop band. In finite structure the attenuation level at these resonance peaks are much lower then neighbouring frequencies which is not possible to notice from the dispersion diagram of infinite structure. This elucidates the importance of identification of natural frequencies while estimating the vibration attenuation performance of the finite structure from the dispersion diagram of infinite structure. By increasing the number of unit RECM cells the attenuation level can be reduced but complete elimination of peak is not possible [35, 36].

4.2 Visualization of wave propagation

The visualisation of flexural wave propagation and attenuation through the RECM beam is only possible in time domain. The Euler Bernoulli beams are dispersive in nature, and the dispersion is proportional to the square root of excitation frequency [37]. The flexural wave of any frequency is able to propagate through an Euler-Bernoulli beam; however, waves containing specific band of frequencies attenuates in case of RECM as discussed in the previous section. To elucidate the wave propagation, here, the following connections between two elastic beams are studied:

1. A uniform Euler-Bernoulli beam having identical properties.
2. Eight elements of RECM with zero rotary inertia ($\psi = 0$), length ratio ($\xi = 0.56$) and mass ratio ($\mu = 0.25$)
3. Eight elements of RECM with non-zero rotary inertia ($\psi = 5$), length ratio ($\xi = 0.56$) and mass ratio ($\mu = 0.25$).

The input displacement controlled wave burst [38] of a particular mid frequency 12.5 Hz and frequency range from 0 to 25, is selected and applied at one end of beam to get the better insight to the physics of wave attenuation because of connecting RECM elements. the time domain results are produced for a input flexural wave pulse as depicted in Figure 9.

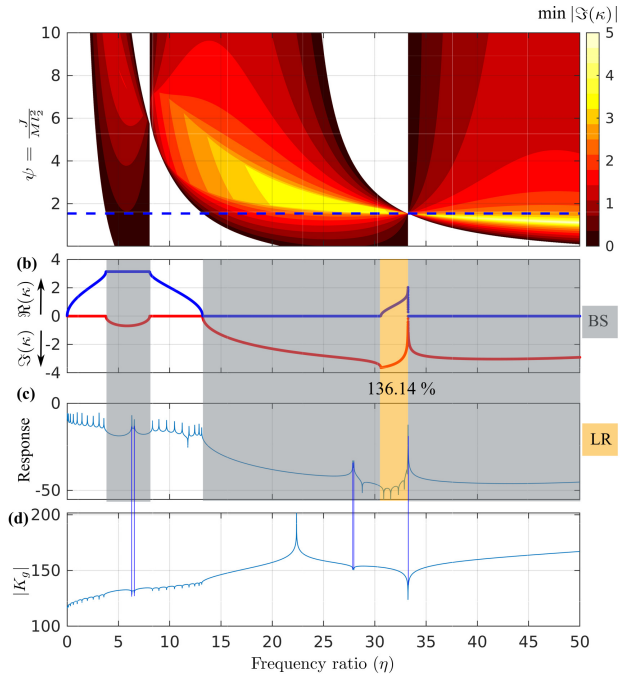

Fig. 8: (a)Attenuation-profile for varying rotary inertia ratio ψ having mass ratio $\mu = 5$ and length ratio $\xi = 0.5$. For the system parameters corresponds to $\psi = 1.71$, $\mu = 0.25$ and $\xi = 0.5$ - (b) concise dispersion diagram illustrating the attenuation and propagation bands and (c) plot of the cross frequency response function evidenced the reduction of response in the attenuation band. The normalised band width of second merged band is 136.14% (d) Plot of logarithmic determinant of global Spectral element Matrix, where downward peak corresponds to the natural frequency of the system. The thin blue lines connecting resonance peaks in (c) and downward peak in (d) illustrate occurrence of resonance peaks in the stop band.

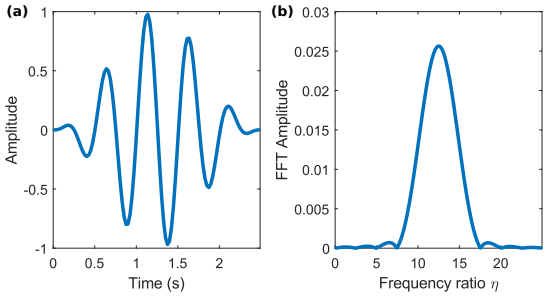

Fig. 9: (a)Input excitation wave burst in time domain (b)Input excitation wave burst in frequency domain

4.2.1 A uniform Euler-Bernoulli beam having identical properties

The wave propagation in space and time domain in case of beams connected with same elastic part can be observed in Figure 10. From Figure 10(a), it can be seen that the input flexural wave is propagating and it is getting dispersed very slowly in time and space. The Figure 10(b) and Figure 10(c) illustrates the nature of wave before and after the connecting element. It can be concluded that flexural waves propagates uninterruptedly through the uniform connecting beam; henceforth, it is not useful for the attenuation of wave.

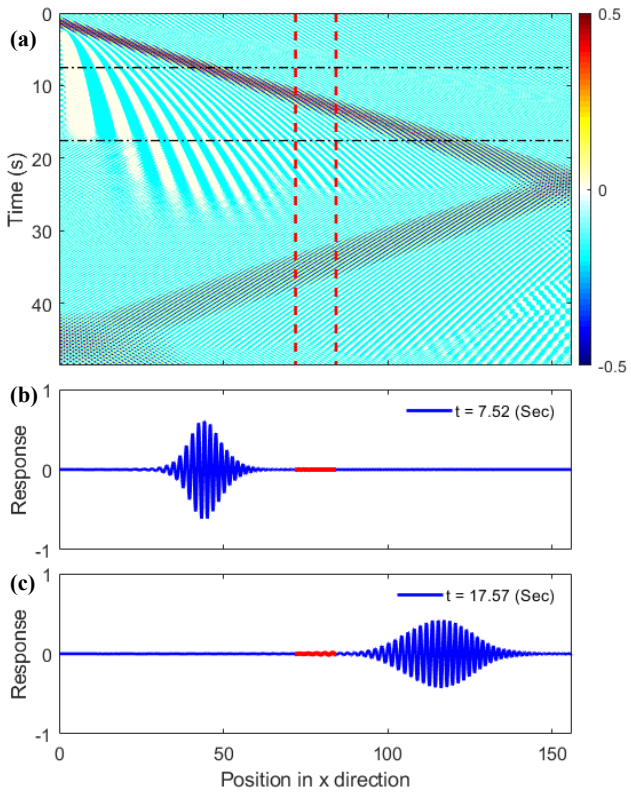

Fig. 10: (a)Wave propagation in space and time (b)snap shot of beam before the wave reaches connecting element (c) snap shot of beam after the wave propagates through connecting element; the red band shows the elastic(same material as of beam) connecting two elastic beams

4.2.2 RECM with zero rotary inertia

Now the connecting elastic part is replaced by eight elements of RECM with zero rotary inertia ($\psi = 0$), length ratio ($\xi = 0.56$) and mass ratio ($\mu = 0.25$). From Figure 5 (b), it can be noticed that the complete excitation frequency band is not falling completely in the band gap, only the end portions of input excitation frequency range is in the stop band. So the large portion of wave should propagate uninterruptedly. From Figure 11, this phenomenon can be observed. part Figure 11(a) shows the excitation wave and the part (b) shows

propagation of the same wave and also the reflection of other frequencies which might be in the stop band.

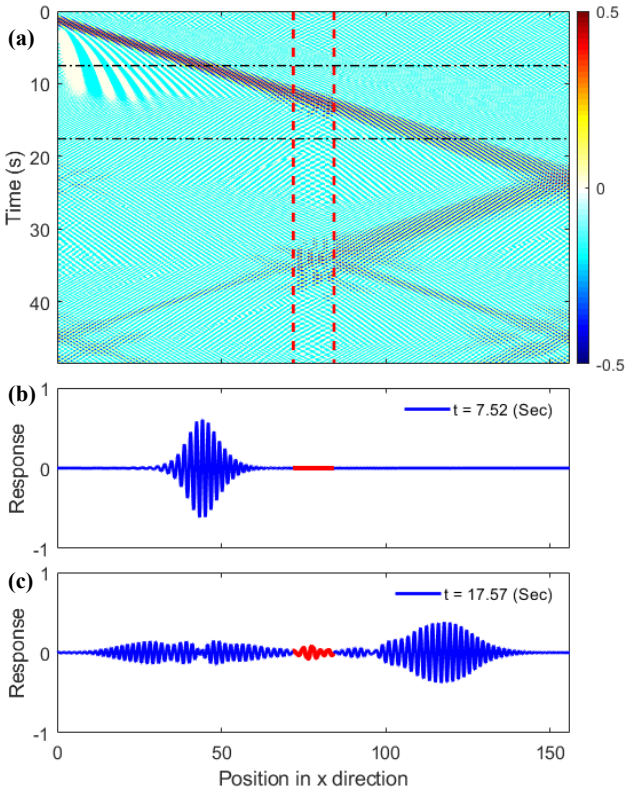

Fig. 11: (a)Wave propagation in space and time (b) snap shot of beam before and (c) after the wave propagates through connecting element; the red band shows the RECM elements with zero rotary inertia- connecting two elastic beams

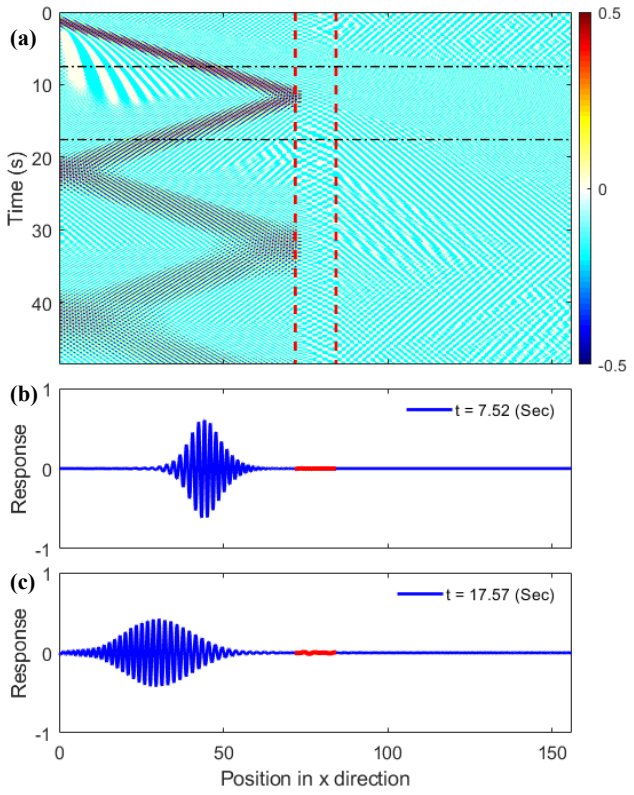

Fig. 12: (a)Wave propagation in space and time (b)snap shot of beam before the wave reaches connecting element (c) snap shot of beam after the wave propagates through connecting element; the red band shows the RECM elements with nonzero rotary inertia- connecting two elastic beams

4.2.3 RECM with non-zero rotary inertia

After introducing the rotary inertia (psi = 5) the wide band gap is achieved by observing the merge of two bragg bands with the LR band as per illustrated in Figure 6. Now, the connecting meta beam is replaced with eight elements RECM with rotary inertia ($\psi = 5$), length ratio ($\xi = 0.56$) and mass ratio ($\mu = 0.25$) and the Figure 11 illustrates complete reflection and zero propagation of incoming wave as the complete frequency range falls under band gap.

5 Conclusion

Spectral element matrix for a rigid elastic combined meta-beam (RECM) is formulated and further the transfer matrix is derived for studying the flexural wave propagation through it. The first three natural frequencies of the unit cell of a RECM obtained from the developed algorithm is validated with the existing state-of the art. Due to the periodic interference of the rigid body, Bragg-bands are observed in the dispersion diagram while the rotary inertia is considered to be zero. The salient feature of this proposed RECM is the emerging LR band in case of nonzero rotary inertia. For few specific cases, this LR band assists to merge both the Bragg band and turns into an ultra-wide stop-band with significant level of attenuation; otherwise also it can widen the attenuation band gap. The sensitivity analysis helps us to predict the parameters for obtaining the desired attenuation profile. The spectral element formulation of rigid-elastic combined beam, observation of LR band without using any resonators are the key contributions of this paper. Specifically, 164% normalized bandwidth can be obtained in RECM. Further, the frequency response function and natural frequencies of the finite RECM is evaluated. It has been noticed that some natural frequencies lies within the attenuation band; henceforth, reduces the level of attenuation at those frequencies. Importantly, this information cannot be obtained from the dispersion plot of the infinite system. Additionally, to comprehend propagation, attenuation and reflection of the dispersive flexural wave burst through an uniform Euler-Bernoulli (EB) beam and finite number of rigid elastic combined meta-beam (RECM) elements sandwiched between two Euler Bernoulli beams are investigated. An in house program is developed to convert the response from frequency domain to the space-time domain employing spectral element matrix, assembly method of finite element method and inverse Fourier trans-

form. Future investigation can be carried out to realize the system in practice. *Acknowledgement*: Authors acknowledge Inspire faculty grant, grant number: DST/INSPIRE /04/2018/000052, for supporting the research.

A Animation videos of visualisation of wave propagation

Animation of wave propagation, attenuation and reflection for

Uniform beam:
"w_12dot5_Elastic_space_displacement_bc.avi"
sandwiched RECM with zero rotary inertia:
"w_12dot5_psi0_RECM_displacement_bc.avi"
sandwiched RECM with non-zero rotary inertia:
"w_12dot5_psi5_RECM_displacement_bc.avi"

References

[1] Mead, D., 1973. "A general theory of harmonic wave propagation in linear periodic systems with multiple coupling". *Journal of Sound and Vibration,* **27**, Mar., pp. 235–260.

[2] Mead, D., 1996. "WAVE PROPAGATION IN CONTINUOUS PERIODIC STRUCTURES: RESEARCH CONTRIBUTIONS FROM SOUTHAMPTON, 1964–1995". *Journal of Sound and Vibration,* **190**, Feb., pp. 495–524.

[3] SenGupta, G., 1980. "Vibration of Periodic Structures". *The Shock and Vibration Digest,* **12**, Mar., pp. 17–31.

[4] Roy, A., and Plunkett, R., 1986. "Wave attenuation in periodic structures". *Journal of Sound and Vibration,* **104**, Feb., pp. 395–410.

[5] Orris, R. M., and Petyt, M., 1974. "A finite element study of harmonic wave propagation in periodic structures". *Journal of Sound and Vibration,* **33**, Mar., pp. 223–236.

[6] Mace, B., 1984. "Wave reflection and transmission in beams". *Journal of sound and vibration,* **97**(2), pp. 237–246.

[7] Brillouin, L., 1953. "Wave propagation in periodic structures: electric filters and crystal lattices". Publisher: Dover.

[8] Mead, D. J., 1970. "Free wave propagation in periodically supported, infinite beams". *Journal of Sound and Vibration,* **11**(2), pp. 181–197. Publisher: Elsevier.

[9] Banerjee, A., Das, R., and Calius, E. P., 2019. "Waves in Structured Mediums or Metamaterials: A Review". *Archives of Computational Methods in Engineering,* **26**, Sept., pp. 1029–1058.

[10] Prasad, R., and Banerjee, A., 2021. "Influence of conicity on the free wave propagation in symmetric tapered periodic beam". *Mechanics Research Communications,* **111**, Jan., p. 103655.

[11] Xiao, Y., Wen, J., Yu, D., and Wen, X., 2013. "Flexural wave propagation in beams with periodically attached vibration absorbers: Band-gap behavior and band formation mechanisms". *Journal of Sound and Vibration,* **332**, Feb., pp. 867–893.

[12] Yuksel, O., and Yilmaz, C., 2020. "Realization of an ultrawide stop band in a 2-d elastic metamaterial with topologically optimized inertial amplification mechanisms". *International Journal of Solids and Structures,* **203**, pp. 138–150.

[13] Liu, L., and Hussein, M. I., 2012. "Wave Motion in Periodic Flexural Beams and Characterization of the Transition Between Bragg Scattering and Local Resonance". *Journal of Applied Mechanics,* **79**, Jan., p. 011003.

[14] Ozmutlu, A., Ebrahimian, M., and Todorovska, M. I., 2018. "Wave propagation in buildings as periodic structures: Timoshenko beam with rigid floor slabs model". *Journal of Engineering Mechanics,* **144**(4), p. 04018010.

[15] Frandsen, N. M., Bilal, O. R., Jensen, J. S., and Hussein, M. I., 2016. "Inertial amplification of continuous structures: Large band gaps from small masses". *Journal of Applied Physics,* **119**(12), p. 124902. Publisher: AIP Publishing LLC.

[16] Yu, D., Wen, J., Shen, H., Xiao, Y., and Wen, X., 2012. "Propagation of flexural wave in periodic beam on elastic foundations". *Physics Letters A,* **376**(4), pp. 626–630.

[17] Xiao, Y., Wen, J., and Wen, X., 2012. "Broadband locally resonant beams containing multiple periodic arrays of attached resonators". *Physics Letters A,* **376**(16), pp. 1384–1390.

[18] Banerjee, A., 2020. "Non-dimensional analysis of the elastic beam having periodic linear spring mass resonators". *Meccanica,* **55**, May, pp. 1181–1191.

[19] Banerjee, A., 2020. "Influence of the torsional vibration of the periodically attached perpendicular beam resonator on the flexural band of a Euler-Bernoulli beam". *Physics Letters A,* **384**, Oct., p. 126757.

[20] Wang, T., Sheng, M.-P., and Qin, Q.-H., 2016. "Multi-flexural band gaps in an Euler–Bernoulli beam with lateral local resonators". *Physics Letters A,* **380**(4), pp. 525–529.

[21] Sugino, C., and Erturk, A., 2018. "Analysis of multifunctional piezoelectric metastructures for low-frequency bandgap formation and energy harvesting". *Journal of Physics D: Applied Physics,* **51**(21), p. 215103.

[22] Banerjee, A., 2021. "Flexural waves in graded metabeam lattice". *Physics Letters A,* **388**, Feb., p. 127057.

[23] Hu, G., Austin, A. C., Sorokin, V., and Tang, L. "Metamaterial beam with graded local resonators for broadband vibration suppression". *Mechanical Systems and Signal Processing,* **146**, p. 106982.

[24] Manohar, C., and Adhikari, S., 1998. "Dynamic stiffness of randomly parametered beams". *Probabilistic Engineering Mechanics,* **13**(1), pp. 39–51.

[25] Lee, U., 2009. *Spectral element method in structural*

dynamics. J. Wiley & Sons Asia, Singapore ; Hoboken, NJ.

[26] Jang, I., and Lee, U., 2012. "Spectral element analysis of the axial-bending-shear coupled vibrations of composite Timoshenko beams". *Journal of Composite Materials,* **46**, Oct., pp. 2811–2828.

[27] Low, K., 1998. "ON THE EIGENFREQUENCIES FOR MASS LOADED BEAMS UNDER CLASSICAL BOUNDARY CONDITIONS". *Journal of Sound and Vibration,* **215**, Aug., pp. 381–389.

[28] Banerjee, J., and Sobey, A., 2003. "Further investigation into eigenfrequencies of a two-part beam–mass system". *Journal of Sound and Vibration,* **265**, Aug., pp. 899–908.

[29] Obradović, A., Šalinić, S., Trifković, D. R., Zorić, N., and Stokić, Z., 2015. "Free vibration of structures composed of rigid bodies and elastic beam segments". *Journal of Sound and Vibration,* **347**, pp. 126–138. Publisher: Elsevier.

[30] Tomović, A., Šalinić, S., Obradović, A., Grbović, A., and Milovančević, M., 2020. "Closed-form solution for the free axial-bending vibration problem of structures composed of rigid bodies and elastic beam segments". *Applied Mathematical Modelling,* **77**, Jan., pp. 1148–1167.

[31] Liu, X., Sun, C., Ranjan Banerjee, J., Dan, H.-C., and Chang, L., 2021. "An exact dynamic stiffness method for multibody systems consisting of beams and rigid-bodies". *Mechanical Systems and Signal Processing,* **150**, Mar., p. 107264.

[32] Wu, J.-J., 2011. "Use of the elastic-and-rigid-combined beam element for dynamic analysis of a two-dimensional frame with arbitrarily distributed rigid beam segments". *Applied Mathematical Modelling,* **35**, Mar., pp. 1240–1251.

[33] Mead, D., 1975. "Wave propagation and natural modes in periodic systems: Ii. multi-coupled systems, with and without damping". *Journal of Sound and Vibration,* **40**(1), pp. 19–39.

[34] Fu, Z.-F., and He, J., 2001. *Modal analysis*. Elsevier.

[35] Banerjee, A., Das, R., and Calius, E. P., 2016. "A new approach for determination of the attenuation bandwidth of a resonating metamaterial". In Applied Mechanics and Materials, Vol. 846, Trans Tech Publ, pp. 264–269.

[36] Davis, B. L., Tomchek, A. S., Flores, E. A., Liu, L., and Hussein, M. I., 2011. "Analysis of periodicity termination in phononic crystals". In ASME International Mechanical Engineering Congress and Exposition, Vol. 54945, pp. 973–977.

[37] Doyle, J. F., 2012. *Wave propagation in structures: an FFT-based spectral analysis methodology*. Springer Science & Business Media.

[38] Huang, H., and Sun, C., 2011. "Theoretical investigation of the behavior of an acoustic metamaterial with extreme young's modulus". *Journal of the Mechanics and Physics of Solids,* **59**(10), pp. 2070–2081.